Australian Government
Department of Defence
Defence Science and
Technology Organisation

A Feasibility Study into the Active Smart Patch Concept for Composite Bonded Repairs

N. Rajic and S. C. Rosalie

Air Vehicles Division
Defence Science and Technology Organisation

DSTO–TR–2247

ABSTRACT

This report describes an experimental investigation into a novel form of composite bonded repair called the Active Smart Patch (ASP). The ASP represents an important conceptual advancement over conventional repair technology by incorporating into a patch a network of embedded piezoelectric elements that provides a diagnostic facility for structural health. This type of repair is being developed as a means of mitigating the strict certification requirements currently placed on bonded repairs to primary aircraft structure, and as a potentially cost-efficient means of providing structural integrity assurance where lack of access precludes conventional nondestructive inspection. Initial development of the concept targets the problem of cracking at Forward Auxillary Spar Station (FASS) 281.28 in the F-111 Lower Wing Skin. As a first approximation to this problem, a prototype ASP was developed and then applied to a metal coupon which was notched to simulate cracking. The study shows that a network of piezoelectric transducers embedded in the bond-line of the patch provides a robust basis for the detection of notch growth.

Published by

Defence Science and Technology Organisation
506 Lorimer St,
Fishermans Bend, Victoria 3207, Australia

Telephone: *(03) 9626 7000*
Facsimile: *(03) 9626 7999*

AR No. 014-394
August 2008

APPROVED FOR PUBLIC RELEASE

A Feasibility Study into the Active Smart Patch Concept for Composite Bonded Repairs

EXECUTIVE SUMMARY

Composite bonded repair technology offers an effective and cost efficient means of remediation for damaged metallic aircraft components, with successful repairs applied to a variety of aircraft including Mirage III, C-141 and F-111. One of the most ambitious applications of the technology was to the repair of cracking at Forward Auxillary Spar Station (FASS) 281.28 in the lower wing skin of the RAAF F-111C aircraft. Involving primary structure and a critical flaw, the use of a composite bonded repair (CBR) in this case was ambitious. It was flight certified only after a stringent analytical and experimental substantiation testing program had demonstrated the airworthiness of the repair. In addition, a rigorous nondestructive inspection regime was mandated for the repaired structure to provide ongoing structural integrity assurance. The repair did prove successful, however the onerous basis for structural certification was seen as a serious impediment to the broader acceptance of CBR's for application to primary aircraft structure.

An integrated diagnostic facility could mitigate these certification requirements by providing ongoing assurance of the structural integrity and performance of the repair. This has led to the development at the DSTO of a repair termed the "Active Smart Patch" (ASP). A diagnostic capability is derived from a network of piezoelectric elements embedded in the bondline. These provide a means of transmitting and receiving acoustic waves which, in principle, can be used to interrogate both the composite patch and the repaired structure. Although the concept is broad in its potential scope of application, the initial development of the ASP targets the specific problem of cracking at Forward Auxillary Spar Station (FASS) 281.28 in the F-111 Lower Wing Skin. A prototype patch was developed and applied to an aluminium coupon in which a circular notch was grown to simulate cracking in the wing skin. Tests showed that notch growth in the coupon could be robustly detected on the basis of measurements obtained from piezoelectric elements embedded in the bondline of the repair.

The demonstration underscores the potential of an integrated network of piezoelectric elements to provide a diagnostic capability for structural components reinforced by a CBR. By promoting wider uptake of a cost efficient means of aircraft structural repair, and furnishing a basis for condition-based structural management, the work represents an important outcome for defence.

Authors

Nik Rajic
Air Vehicles Division

Nik Rajic received a B. Eng. (Hons.) in Mechanical Engineering from the University of Melbourne in 1989. He joined Structures Division at the Aeronautical Research Laboratory in 1991 and in 1992 undertook studies at Monash University which led to the completion of a PhD in 1995. He has since contributed to research on fatigue-life extension techniques, thermoelastic stress analysis, thermoplasticity, thermographic nondestructive evaluation, and in situ structural health monitoring techniques based on smart structures principles. He is currently a Senior Research Scientist in the Air Vehicles Division.

Stephane C. Rosalie
Fortburn Consulting

Stephane C. Rosalie received a B. Eng. (Hons.) in Mechanical Engineering from Monash University in 2002. Further study at Monash University led to the completion of a PhD in 2006. He is currently employed by Fortburn consulting and is contracted to the Air Vehicles Division in the Smart Structures and Advanced Diagnostics group

Contents

Appendices

Figures

1 Introduction

Composite bonded repair (CBR) technology offers an effective and cost efficient means of restoring damaged aircraft components. An example is the boron epoxy patch developed to repair cracking in the lower wing skin (LWS) of the F-111C aircraft [1]. A stiffener depression at Forward Auxillary Spar Station (FASS) 281.28 conceived in design to facilitate fuel flow through the wing was, in practice, found to promote early crack growth rendering the wing unserviceable. The application of a composite bonded repair in this situation was considered ambitious since it involved critical damage to primary structure. The repair was flight certified only after a comprehensive analytical and experimental substantiation testing program [2] had demonstrated its airworthiness. In addition, a rigorous nondestructive inspection regime was mandated for the repaired structure to provide ongoing assurance of structural integrity. The repair did prove successful, however the onerous basis for structural certification was seen as a serious impediment to the broader acceptance of CBR technology for application to primary aircraft structure.

The concept of an intelligent or smart structure offers a promising basis for mitigating structural certification requirements for composite bonded repairs. In particular, a network of low-profile piezoelectric transducers embedded in the bond-line of the patch could provide a basis for certifying the durability of the repair. This approach offers a useful advancement in structural health monitoring capability over that of the "Smart Patch" device described in [3] and successfully flight trialled in 2006 on an F/A-18 Aileron Hinge. The Smart Patch employed conventional electrical resistance foil gauges and PVDF (polyvinylidene) piezoelectric film to sense the local strain relaxation that occurs in response to failure of the bondline. However, the success of the approach is contingent on the accurate placement of strain sensors, which assumes an a priori knowledge of where patch failure will occur. This limits its scope of application. By comparison, piezoelectric elements provide for much broader diagnostic coverage. Elastic waves produced by these elements can propagate over relatively large distances in structural wave guides like wing skins and thus permit genuine remote inspection. As an extension of the original Smart Patch [3] concept, this new repair is termed the "Active Smart Patch" (ASP).

The development of an ASP for an aircraft application like the F-111C wing skin repair is a multidisciplinary undertaking, relying on an integration of materials, microelectronics, signal processing and sensor packaging technologies. Efforts are currently underway in each of these areas, however in an attempt to clarify the key engineering issues and to test the feasibility of the concept in general, it was thought useful to conduct an initial proof-of-concept study based on a simple laboratory demonstrator. This report outlines work on the development of a prototype repair and an experimental evaluation of the diagnostic value of low-profile piezoelectric elements embedded in the bond line.

It can be argued that the primary diagnostic focus of a structural health monitoring (SHM) system embedded in a patch should be on the bondline, since it is the inability to provide assurance of bondline strength that is the primary source of certification concerns. In the F-111 LWS however, another key objective of SHM is to provide a basis for continuous monitoring of cracking in the damaged wing structure. The two goals are not entirely separate since a reduction in patching efficiency caused by partial failure of the bondline should lead to an increased rate of crack growth. The value of a diagnostic capability

for cracking in the host is also more immediate since it potentially makes redundant the requirement for costly ongoing manual nondestructive inspection (NDI) of the repaired wing structure.

Compared to bond-line degradation, cracking of the wing skin is a simpler diagnostic problem and more amenable to systematic investigation since the nature and location of the damage is known. For these reasons the study targets only this problem. In a further simplification of the diagnostic problem, a crack in the parent structure is simulated by a circular notch formed with a high-speed disc cutter. The mechanical loading required to grow a genuine crack would expose the piezoceramic elements to a risk of structural failure and thereby complicate diagnostic assessments. Issues relating to the mechanical durability of piezoceramic elements are treated only briefly in this report, as a separate detailed study addressing this subject will be reported elsewhere.

2 Experimental Procedure

Two metal coupons were formed by cutting 400 mm lengths from 6060-T5 aluminium alloy rectangular bar stock 6.2 mm thick and 32 mm wide. One coupon was patched while the other remained unpatched to serve as a benchmark. On the latter sample, four square PZT-5A piezoelectric elements with a side dimension of 10 mm and 250 μm thick were adhesively bonded using a thin layer of heat-cured silver-loaded epoxy (see Figure 1). An electrical connection was made by soldering a lead wire directly to each element.

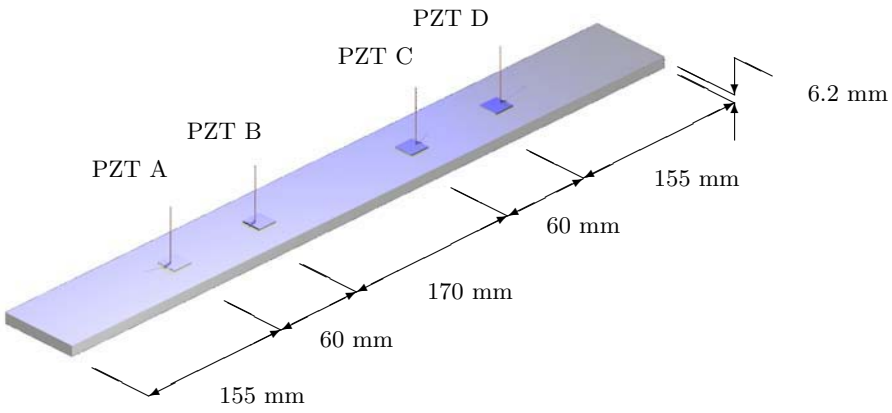

Figure 1: *Schematic of unpatched aluminium coupon showing location of surface mounted piezoelectric elements.*

2.1 Prototype Active Smart Patch

In producing the prototype patch no effort was made to replicate the precise composition and lay-up of the actual F-111 repair patch. Other than the total patch thickness, these factors were not considered critical to an assessment of concept feasibility, and as such the patch was produced using available material. Carbon-fibre prepreg was used in a quasi-isotropic lay-up: $[+45, 0, -45, 90]_{2s}$, to produce a patch approximately 2 mm thick. Accommodation for two piezoelectric elements, each square with a side dimension of 10 mm and 250 μm thick, was made in the patch by positioning dummy elements on the caul plate prior to lay-up. These elements were sufficiently thick to ensure that with the piezoelectric transducers installed the adhered face of the composite patch would be near flush.

To facilitate a durable electrical connection to the piezoelectric element, copper shims 50 μm thick were bonded to the piezoelectric element using DP460 epoxy. The ground-plane shim was extended beyond the perimeter of the piezoelectric element to enable a ground wire to be installed on the piezoceramic side of the shim thereby leaving a clean profile on the adhered face of the patch. The layered assembly was clamped during cure to ensure a good electrical connection.

The cured elements were bonded to the patch using DP460 epoxy adhesive and a layer of scrim cloth to control the bondline thickness. A small hole drilled through the patch allowed for egress of the lead wires. Figure 2 shows the element installed in the patch.

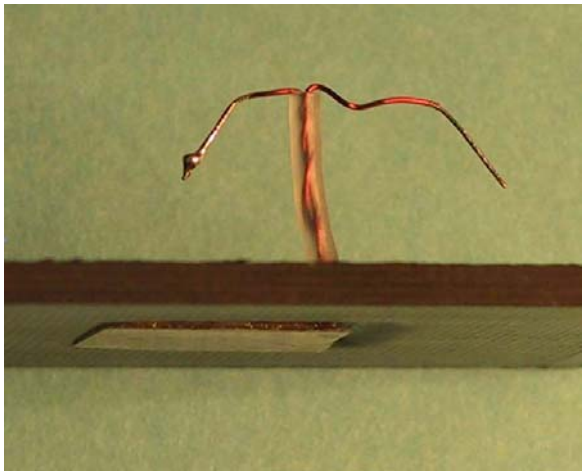

Figure 2: *Underside of Active Smart Patch showing embedded piezoelectric element.*

When bonded in place, the piezoelectric element sits about 100 μm proud of the patch surface. This makes an allowance for the thickness of film adhesive used to bond the patch to the coupon so that when the patch is installed the bondline between the transducer and the coupon is as thin as possible. At the completion of testing, the installed ASP was sectioned to reveal the structure of the adhesive layer adjacent to the piezoelectric element. Figure 3 confirms a bond-line thickness between the piezoelectric element and metal host of under 20 μm. In focusing the diagnostic role of the patch on the detection of cracking in the parent, the production of a thin transducer bond-line was considered important in fostering good coupling of energy into the host. Transfer of energy into the patch is, in

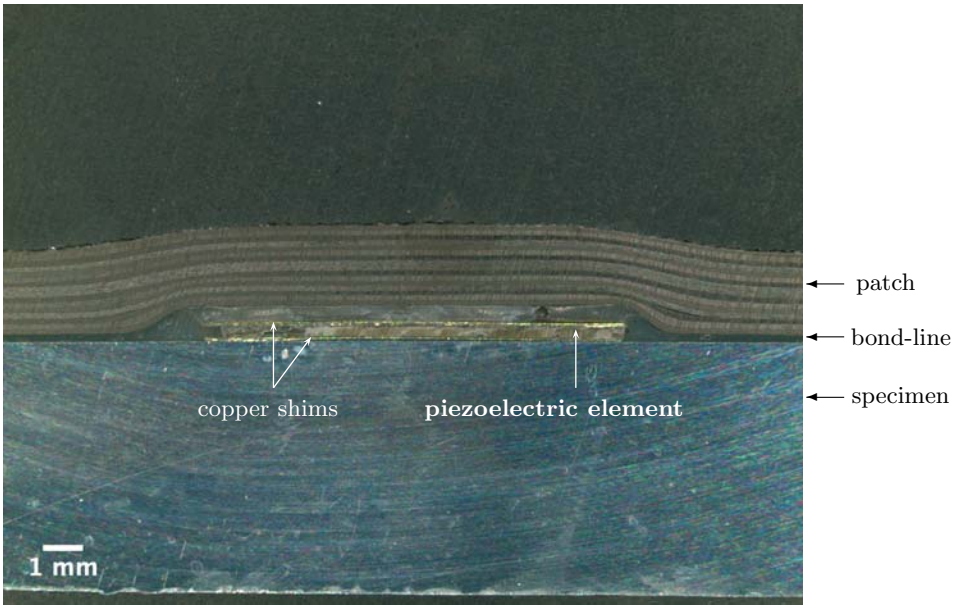

Figure 3: *Sectioned view of reinforced coupon showing bond-line structure adjacent to embedded piezoelectric element.*

this context parasitic, but is fundamental to diagnostic inspection of the adhesive bond line and patch, a problem not considered in the present study.

Fatigue cracking in the metal coupon was simulated by introducing a circular notch on the unpatched side of the sample using an abrasive disc cutter approximately 32 mm in diameter and 1 mm thick.

In addition to the two elements embedded in the patch, a further two elements were fixed to the beam outside of the reinforced section (Figure 4) to match the element placement shown in Figure 1.

2.2 Structural Interrogation

An Acousto-Ultrasonic (AU) [4] arrangement is used to interrogate the coupon. The approach relies on scattering of elastic waves transmitted between piezoelectric elements to reveal structural damage in the wave path. An important advantage of the approach is its good diagnostic range in structural components, like a wing skin, that are 'thin' in comparison to the wavelengths of low frequency ultrasound, and therefore act as efficient waveguides.

The piezoelectric elements are controlled through a device called the AUSAM (Acousto Ultrasonic Structural health monitoring Array Module), developed through a collaborative effort between the DSTO and local industry. Shown in Figure 5, the module provides for autonomous control of two send and four receive elements, and can operate synchronously with other modules to accommodate larger transducer numbers. Communication with the device occurs via a USB link to a computer, which also provides electrical power to the

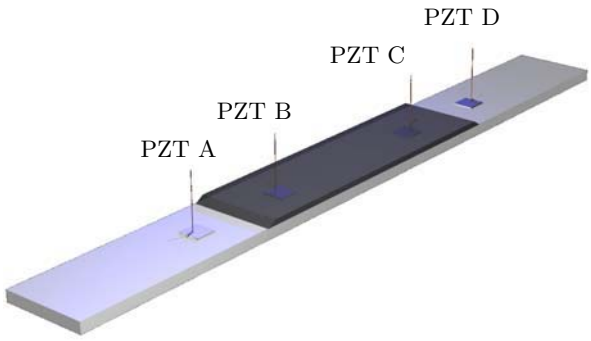

Figure 4: *Schematic of aluminium test coupon with an installed ASP.*

device. Amplifiers on the module can drive typical piezoelectric capacitive loads ($1-10\,\mathrm{nF}$) at near $100\,\mathrm{V}$ to frequencies beyond $2\,\mathrm{MHz}$.

Several transmit/receive pairings were considered in the study to allow for an examination of the impact of embedment on the transduction characteristics of the piezoelectric elements in the patched coupon. The four configurations are:

(1) **SASS**: Surface Actuation (PZT A) & Surface Sensing (PZT D)
(2) **SAES**: Surface Actuation (PZT A) & Embedded Sensing (PZT C)
(3) **EASS**: Embedded Actuation (PZT B) & Surface Sensing (PZT D)
(4) **EAES**: Embedded Actuation (PZT B) & Embedded Sensing (PZT C)

In the absence of a priori knowledge of the structural wave dynamics in the sample, an arbitrary selection of source frequencies were considered in the study, specifically: 50, 125, 200, 300, 400, 500, 600, 700, 800, 900, and $1000\,\mathrm{kHz}$. The drive signal comprised a Hanning modulated tone-burst of 5 cycles with an amplitude of between $10-20\,\mathrm{V}$.

2.3 Baseline tests

In the context of identifying characteristics in a measured signal that indicate structural change, it is critical that an account is taken of the contribution of noise and bias in the measurement. To this end, a sensitivity study was undertaken to establish the extent of natural variation in the response in the sample due to ambient temperature fluctuations and other sources of signal variation. The establishment of a stable baseline response is indeed central to in-situ structural health monitoring (ISHM) which allows for structural

Figure 5: *AUSAM board shown with smaller signal conditioning circuit.*

health assessments to be made on a comparative basis. That is, in contrast to conventional NDI practice which relies on absolute measurements, ISHM permits a differential measurement and consequently provides fundamental noise mitigation advantages.

For both samples, the AUSAM was configured to acquire periodically the receiver response signals over a duration of several days, during which the ambient temperature varied from approximately 19 °C to 27 °C. The measured acoustic response signal was reduced using a wavelet transform [5] to a measure of the peak power in the dominant wave packet, with boundary reflections excluded from the analysis by applying an appropriate time gate.

The results for both samples appear in appendix A. In general, the data indicates a stable baseline response with little variation as a function of ambient temperature, although the 300 kHz case provides an exception for some configurations. For instance, the SASS configuration for the patched specimen yields a 50 percent variation in signal power. The precise cause is unknown but probably relates to the close proximity of this frequency to the first harmonic of the fundamental lateral resonance of the element.

2.4 Notch Growth Tests

A notch was initiated on the free face of the beam, approximately mid way between the inner elements. For both patched and unpatched samples, the notch was created using a high-speed abrasive disc, 32 mm in diameter and 1 mm thick, driven into the specimen in small steps using a precision linear stage (see Figure 6). AU interrogations were made after each cut. The frequency range, excitation level and transducer configurations were unchanged from the baseline test described earlier. The process was repeated over a range of notch depths (see Figure 7). Measurements of the ambient temperature were taken at each step to identify any correlated variations in the acoustic response signal.

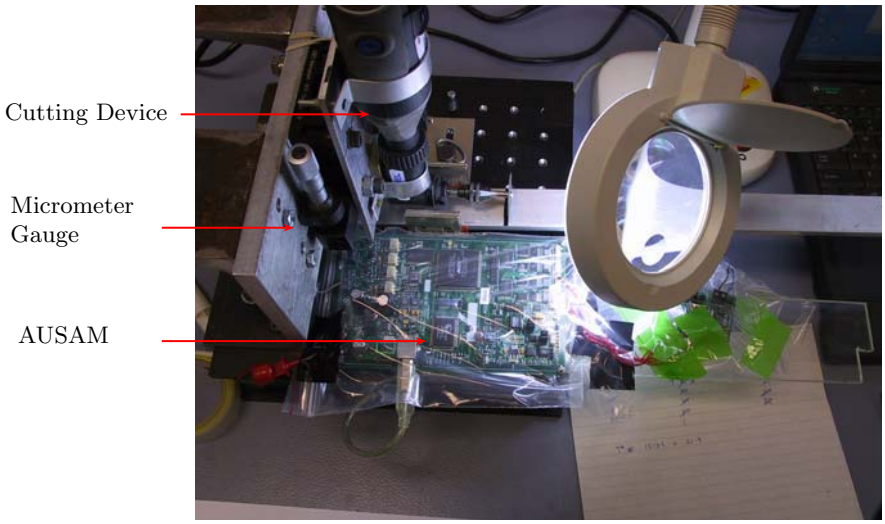

Figure 6: *Formation of notch in beam test specimen (composite patch is on underside of beam).*

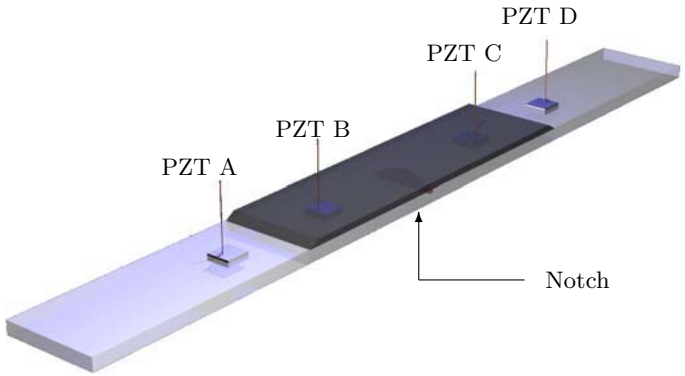

Figure 7: *Schematic of ASP-reinforced metallic coupon showing notch located centrally between inner piezoelectric elements.*

2.5 Scanning Laser Vibrometry

To aid in the interpretation of the piezoelectric sensor measurements, laser vibrometry (LV) was applied to the samples to image the acoustic wave field. Figure 8 shows the scanning system with the main components labeled. The system consists of: (i) a Polytec scanning laser vibrometer (PSV 300), (ii) a two-channel high speed (50 MHz) analogue to digital converter card (ADC) and (iii) a two-axis high-precision linear stage, all controlled by software developed by the DSTO.

The interrogating beam of the vibrometer was aligned perpendicular to the face of the

specimen to detect the out-of-plane (OOP) component of the surface velocity. Both the composite and metal faces of the patched sample were scanned, while on the unpatched sample scanning was done on the face containing the piezoelectric elements.

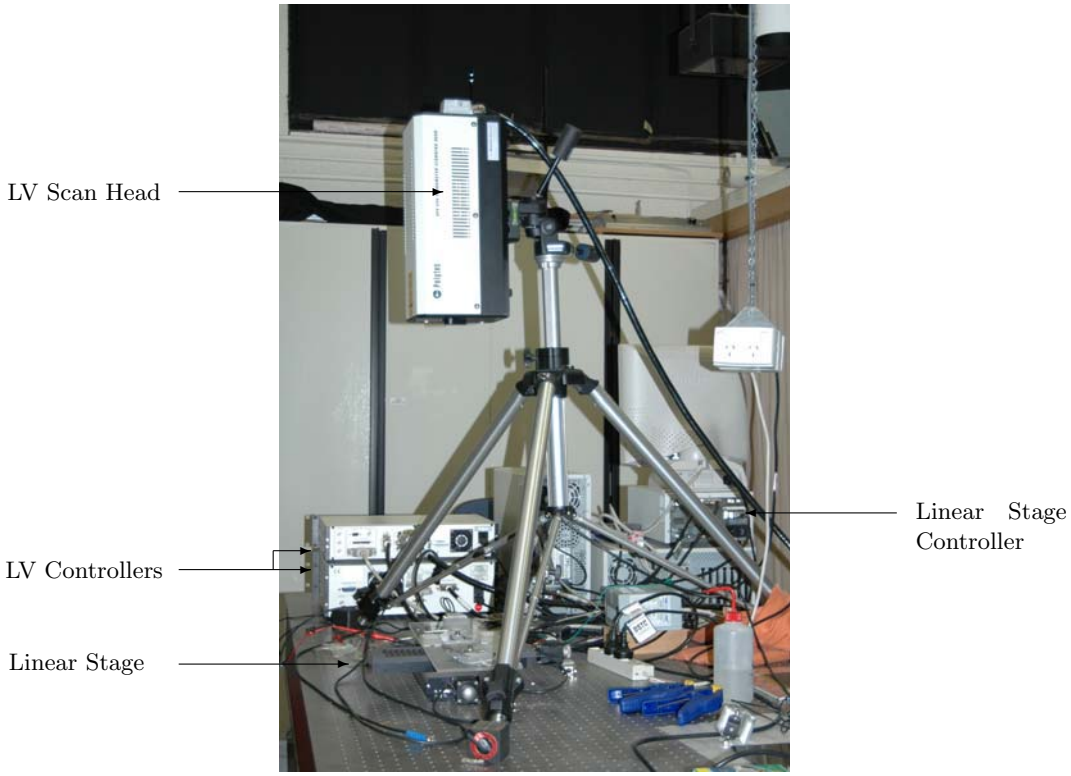

Figure 8: *Laser vibrometry scanning facility.*

3 Results and Discussion

3.1 Unpatched Aluminium Plate

Notch Growth Tests

Representative traces of the piezoelectric response signal in the SASS configuration for the reference and 4.2 mm notch-depth cases are shown in Figures 9(a) and (b), respectively. The disturbance observed at approximately 50 μsecs in the figure corresponds to the drive signal and is inductively coupled. The first genuine acoustic disturbance arrives after a delay of about 60 μsecs. Laser vibrometry was later able to confirm that the responses shown in Figure 9 comprise a mix of guided-wave modes. Multi-modal signals are generally avoided in standard NDI applications because of the difficulty they pose for diagnostic evaluation. However, in the SHM context signal complexity is less of a concern as the diagnostic evaluation is undertaken on a differential basis. Indeed, the presence of a large number of modes in the interrogating wave packet is an advantage since some modes are

likely to be more informative than others. Ideally, a diagnostic evaluation would focus on the more informative constituent modes, however since the modes cannot be isolated on the basis of a single piezoelectric response measurement, a more straightforward approach to signal interpretation must be taken. In this study, variation in the peak signal power in the primary wave packet was taken as a metric for structural change. The power was computed directly from a wavelet transform (Figure 10) of the time signal. A time-gate was applied to the data to exclude boundary reflections.

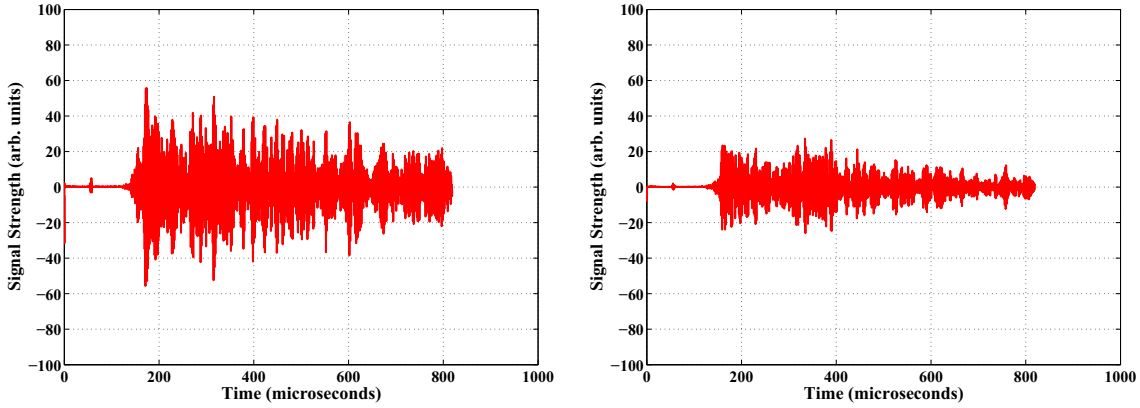

(a) *(b)*

Figure 9: *Signal time-history (SASS - 600 kHz) for the (a) unnotched unpatched specimen and (b) the unpatched specimen with a 4.2 mm deep notch.*

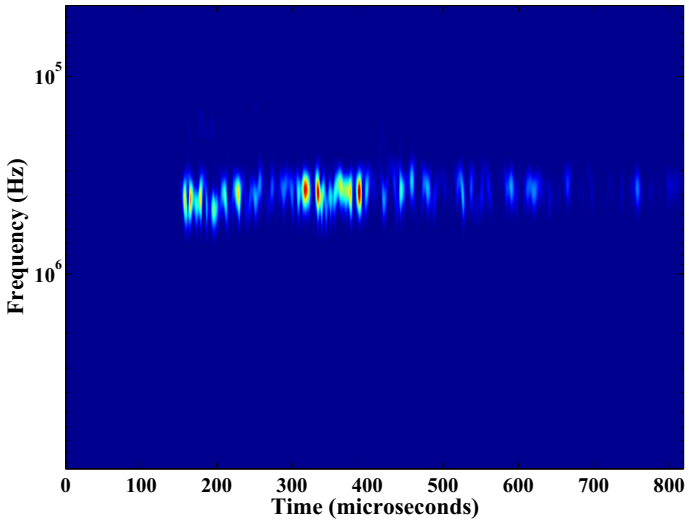

Figure 10: *Wavelet transform of signal time history (SASS - 600 kHz) for the unpatched specimen with a 4.2 mm deep notch.*

Plots of the variation in signal power as a function of notch depth for the eleven considered drive frequencies and four transducer configurations are shown in Appendix B. Overall, an increase in notch depth produces a decline in signal power, which accords with a simple mechanism of acoustic shadowing caused by the notch. The decline however

is non-monotonic, suggesting the presence of more complex wave dynamics. Figure 11 illustrates the non-monotonic decline in signal power. While wave scattering from the notch is likely to account for a large part of the observed growth in signal at shorter notch lengths, experimental noise may also play a role. One influence may have been the repeated removal and reinstallation of the specimen in the notch growth test rig (see Figure 6) which was done to facilitate the vibrometry (see Figure 8). Since piezoelectric elements rely on an applied potential to generate acoustic waves in the parent structure, disturbance of the electrical connections could influence the load impedance and impact on the measurements.

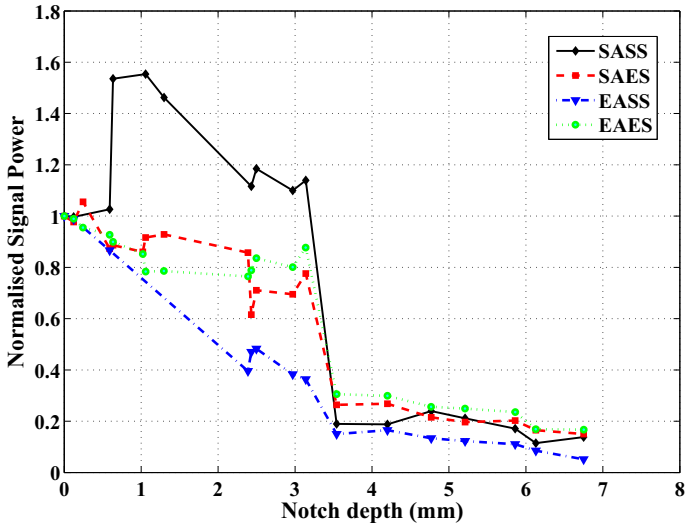

Figure 11: *Signal power measurements for the unpatched specimen at a 600 kHz drive frequency.*

Laser Vibrometry Scans

The samples were examined using laser scanning vibrometry for acoustic drive frequencies of 300 kHz and 600 kHz. Scans were taken at various stages of notch growth in a region between the inner piezoelectric elements, PZT's B and C (see Figure 1). A rectangular area was scanned, approximately 32 mm × 150 mm in size and was sampled at an interval of 1 mm. The response recorded at each sampled point was synchronously averaged to reduce noise. A further improvement in signal to noise ratio was realised by applying a thin retro-reflective film to the surface to enhance reflectivity. The retro-reflective material was found to have no measurable impact on the wave dynamics. The results are presented in Figures 12 and 13 for LV scans at 300 kHz and 600 kHz, respectively.

Figures 12 and 13 show the effect of the notch on wave propagation at the aforementioned frequencies for notch depths of 1.30, 2.36, 3.14, 5.86 and 6.75 mm, respectively, with the latter depth corresponding to complete penetration of the sample. The notch is identified in the LV scans by a framed box representing the size of the notch on the back surface. The scans depict the wave-field at approximately the same time. While a change in the wave-field is noticeable at each notch depth, the 3.14 mm case seems to represent a

transition where the wave front downstream of the notch loses its planar structure. This coincides with a decline in signal recorded in the AU measurements shown in Figure 11.

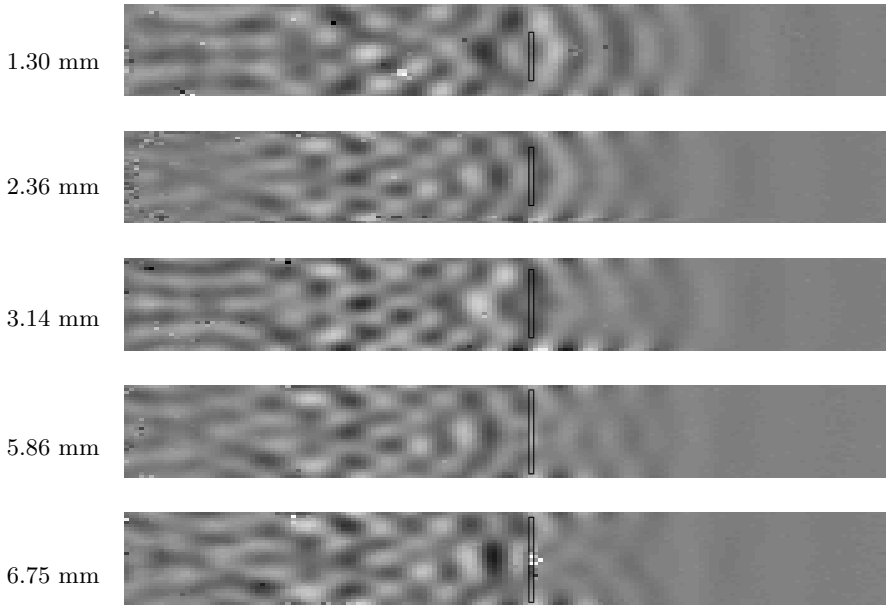

Figure 12: *Effect of notch depth on the acoustic wave field at 300 kHz in the unpatched specimen.*

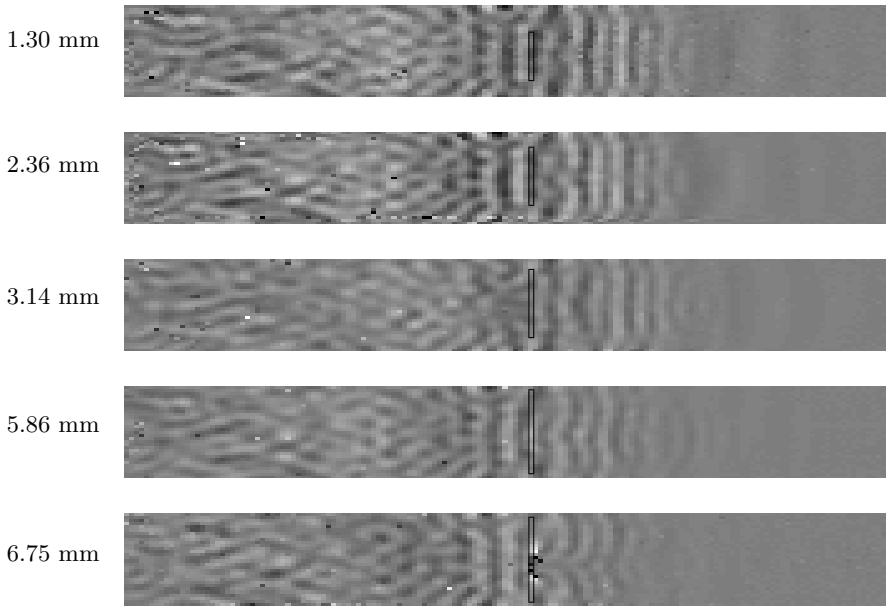

Figure 13: *As in figure 12 but for a 600 kHz drive frequency.*

The spatially resolved nature of the vibrometry data enables the constituent modes in the wave-field to be deduced from a Fourier transform [6]. Transforms were applied

separately to data from the actuator and receiver sides of the notch to isolate mode conversion processes. The analysis was done for piezoelectric drive frequencies of 300 kHz and 600 kHz, and the results combined. Figure 14 shows the outcome for the case of a 1.3 mm deep notch. The results were normalised with respect to the peak magnitude of the spectral decomposition in the upstream region for the respective excitation frequency. The processed experimental data is compared to theoretical dispersion curves for both Lamb waves and horizontally polarised shear waves in the layer defined by the width dimension of the plate [7]. A comparison of the modal content on either side of the notch reveals a general decline in energy across all modes, but in particular the second symmetric and first antisymmetric modes, which are largely extinguished. No additional modes are formed. Appendix C includes similar comparisons for larger notch depths.

That structural damage has a selective impact on certain modes is not unexpected as the displacement fields for some modes will invariably promote greater interaction with a particular flaw geometry. This is desirable from the viewpoint of developing a robust inspection methodology, as it offers a basis for designing an excitation regime that targets only the most informative modes.

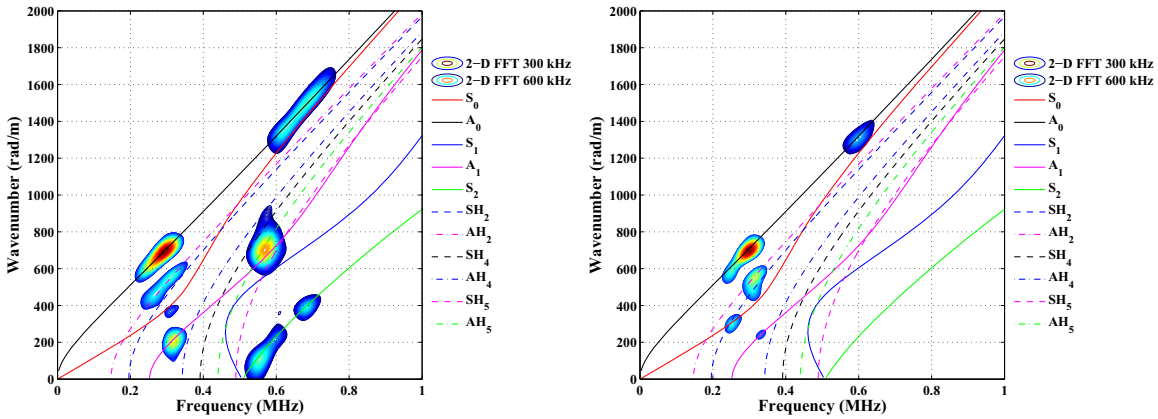

Figure 14: *Comparison of theoretical and measured dispersion characteristics for the unnotched aluminium plate, upstream (left) and downstream (right) of the notch.*

3.2 Patched Aluminium Plate

Notch Growth Tests

The test procedure for the patched coupon was largely a repeat of that for the unpatched variant with one exception. To provide a more stable test environment laser vibrometry was undertaken only after the notch had been grown to its final depth. Representative evolutions of the piezoelectric voltage in the SASS configuration for the reference and 5.1 mm notch-depth cases are shown in Figures 15(a) and (b), respectively. As mentioned previously, the first disturbance relates to the excitation event and is inductively coupled into the receive channel of the AUSAM device. The first acoustic disturbance arrives roughly 60 μs afterwards, followed by a series of larger wave packets. Both the strength and form of the response signal is profoundly affected by the notch, as evidenced by the trace in Figure 15(b).

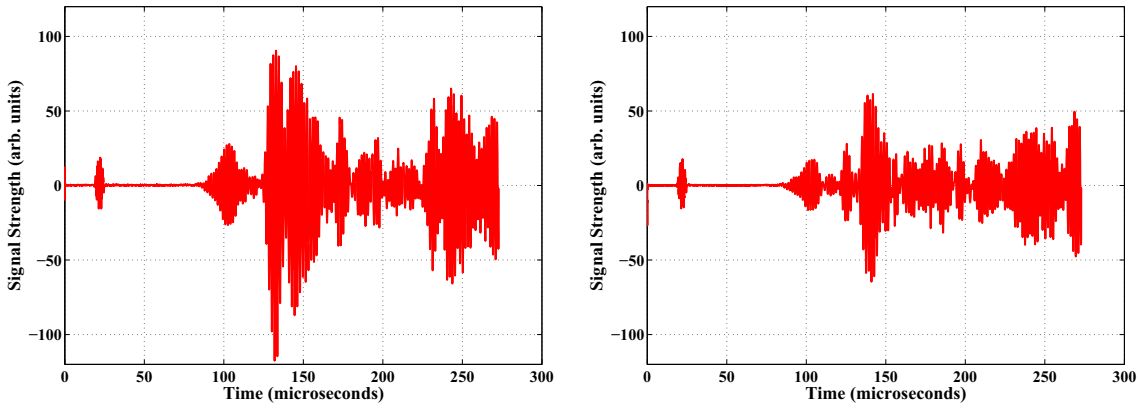

(a) *(b)*

Figure 15: *Signal trace recorded for the following cases: (a) no notch, and (b) a 5.1 mm deep notch (SASS - 600 kHz).*

A complete listing of results for the four transducer configurations is given in Appendix B. Figure 16 condenses these results for the 600 kHz case. All of the transducer configurations reveal substantial variations in signal power compared to background fluctuations (see appendix A) and therefore provide a useful level of sensitivity to notch growth. The EAES case reflects the intended practical implementation of an active smart patch and accordingly represents the most important configuration. It also produces the most complex signal evolution. The first 4 mm of notch growth leads to an increase in signal transfer, and the next 2.5 mm to a decrease. In this situation, if the signal evolution is not tracked at a sufficient frequency the signal power will clearly not furnish a unique estimate for notch length. The capacity to accommodate such complexity represents one of the advantages of a continuous monitoring regime.

The key aspect of the comparison is that neither the presence of the patch nor the embedment of the transducers has impaired detection of notch growth in the sample. It is interesting to note that a notch depth of only 1.6 mm produces a change in signal power of 20%. While changes of at least this order were observed in relation to the unpatched

coupon, the greater stability in the case of the patched sample makes it a more convincing result. As detailed earlier LV scans were made only after growing the notch to its final depth, and the absence of repeated experimental disruption may have contributed to the cleaner response.

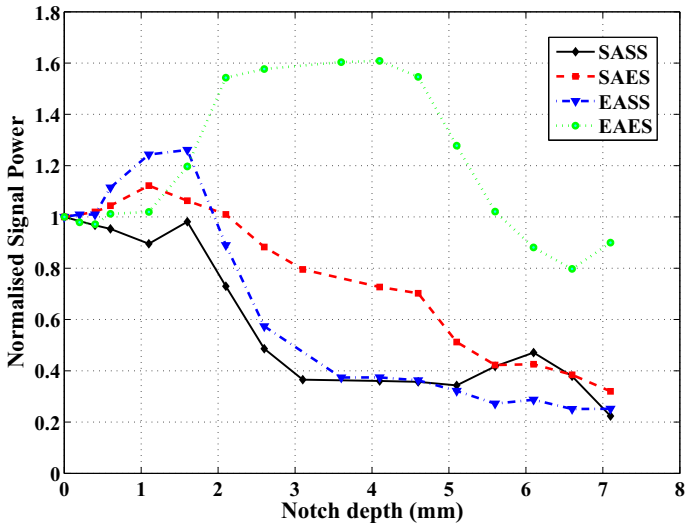

Figure 16: *Variation in signal power as a function of notch depth for the patched coupon at a 600 kHz excitation frequency.*

Laser Vibrometry Scans

Raster scans were formed for the patched sample for narrow-band excitations applied to PZT B at centre frequencies of 300 kHz and 600 kHz. Both the patched and unpatched faces were inspected. Figures 17 and 18 relate to the unpatched surface and 19 and 20 to the patched.

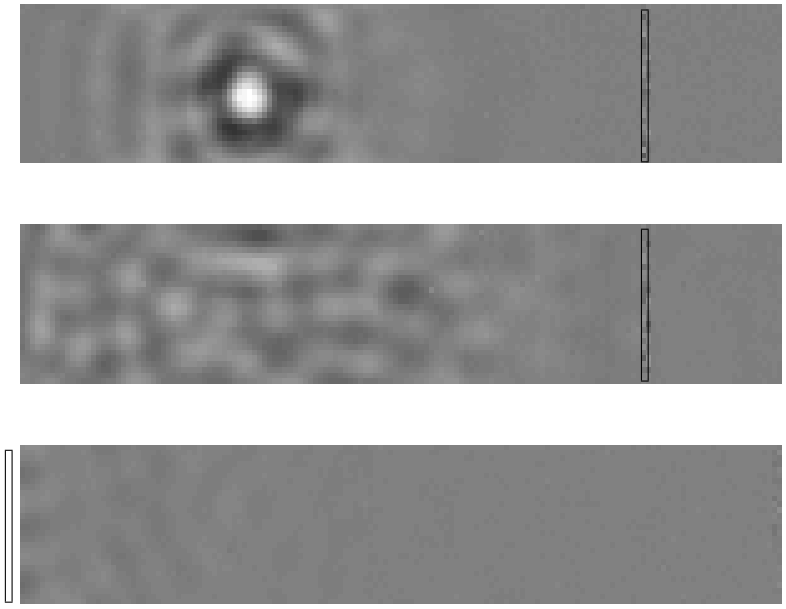

Figure 17: *LV scan of the unpatched surface of the notched ASP coupon for a 300 kHz excitation frequency. Taken a short instant after excitation of PZT B (top), prior to incidence with notch (middle), and after incidence with notch (bottom).*

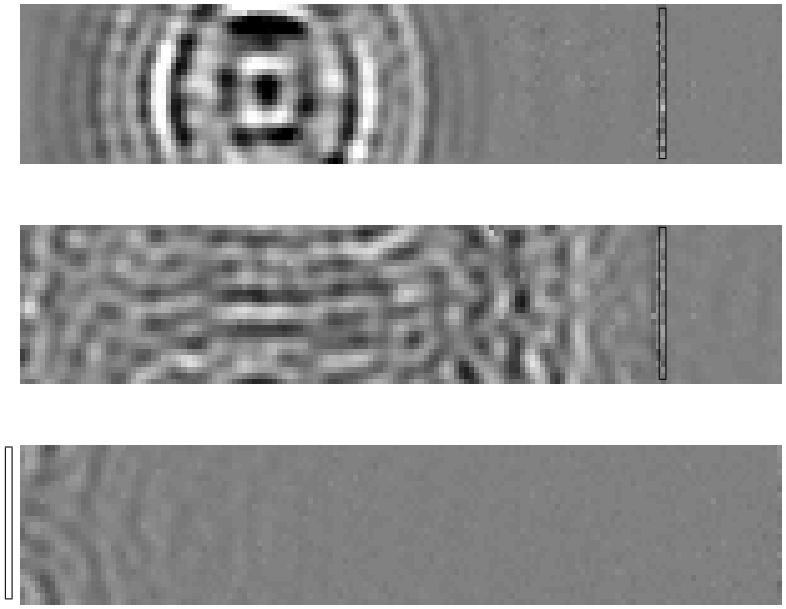

Figure 18: *As in Figure 17 but for a 600 kHz drive frequency.*

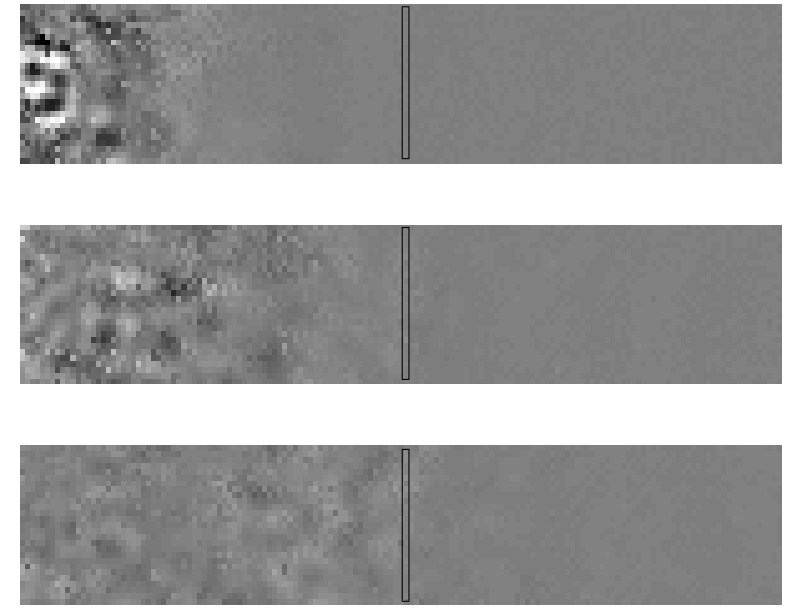

Figure 19: *As in Figure 17 but for the patched surface.*

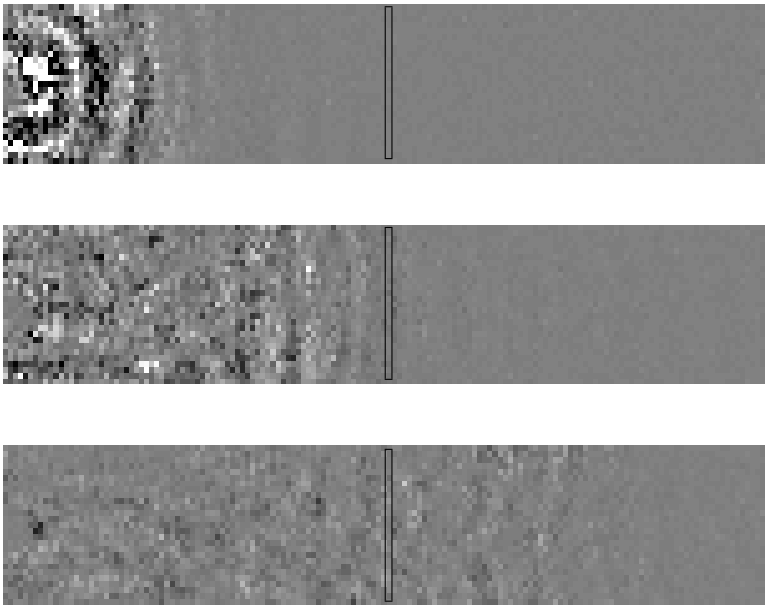

Figure 20: *As in Figure 19 but for a 600 kHz drive frequency.*

The scans reveal strong reverberation between the lateral boundaries of the sample that generally obscures the effect of the notch on the wave-field, although some evidence of interaction appears in Figure 18 as scattering from the edges of the notch. The influence of the notch is more readily observed in a spectral decomposition of the data, which isolates the modal composition of the wave-field on either side of the notch. Before considering this analysis, it is worthwhile briefly remarking on the higher noise levels observed on the patched side of the sample (Figures 19 and 20). The most likely cause is that the rough surface texture of the laminate prevents uniform adhesion of the retro-reflective film, leaving regions of the film unsupported and thereby free to vibrate independently of the substrate.

The layered structure of the reinforced coupon involves several waveguides which need to be considered. Three structures were considered in the analysis: (1) the aluminium substrate, (2) the composite patch, and (3) the aluminium substrate and composite patch. The computed dispersion curves are compared to the decomposed LV data for the unpatched side in Figure 21. Unfortunately, the discrepancy between predicted and measured characteristics is large and precludes a precise and complete identification of all observed modes. The discrepancy is thought to be caused by inaccuracies in the mechanical properties assumed for the composite patch. Where good modal separation occurs, the origin of an observed characteristic can be traced, like for example the mode at 600 kHz and a wavenumber of $450\,\mathrm{rad\,m^{-1}}$, which appears to correspond to Mode_4, a coupled mode. Strong evidence is found in the measured response of a large S_2 component in the metal coupon, uncoupled from the composite patch. However, the mode appears to have been influenced by the patch system since its wavenumber is lower than was observed for the equivalent unpatched coupon (Figure 14). The presence of an uncoupled mode is a useful result as it provides a basis for targeted inspection of the metal substrate. To this end, the S_2 mode appears to be highly sensitive to damage in the substrate, evidenced by its absence in the response downstream of the notch. Although all of the observed modes have been affected by the notch, the effect on S_2 is especially profound given its original strength. This accords with observations in relation to the unpatched coupon (Figure 14), where the S_2 mode was amongst the most informative with regard to notch growth.

Figure 22 shows the equivalent comparison for data gathered from the patched face of the sample. Fewer modes are extinguished compared to the unpatched side, which is to be expected since the notch was confined to the metal substrate.

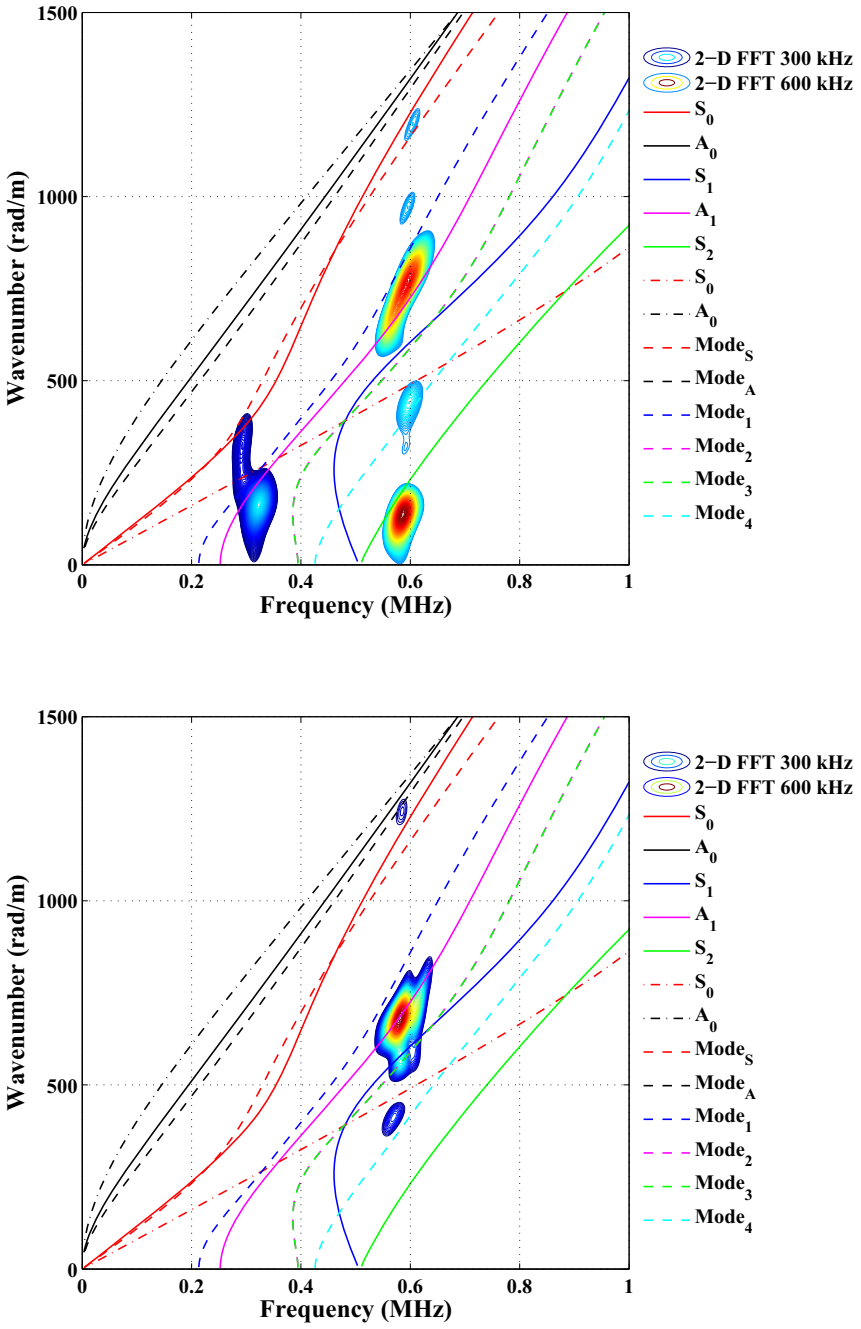

Figure 21: *Spectral decomposition of vibrometry data pertaining to the unpatched face of the coupon, upstream (top) and downstream (bottom) of a through-thickness notch in the metal coupon. Solid lines correspond to modes in the metal coupon, dot-dashed lines to modes in the patch, and dashed lines to modes in the combined structure.*

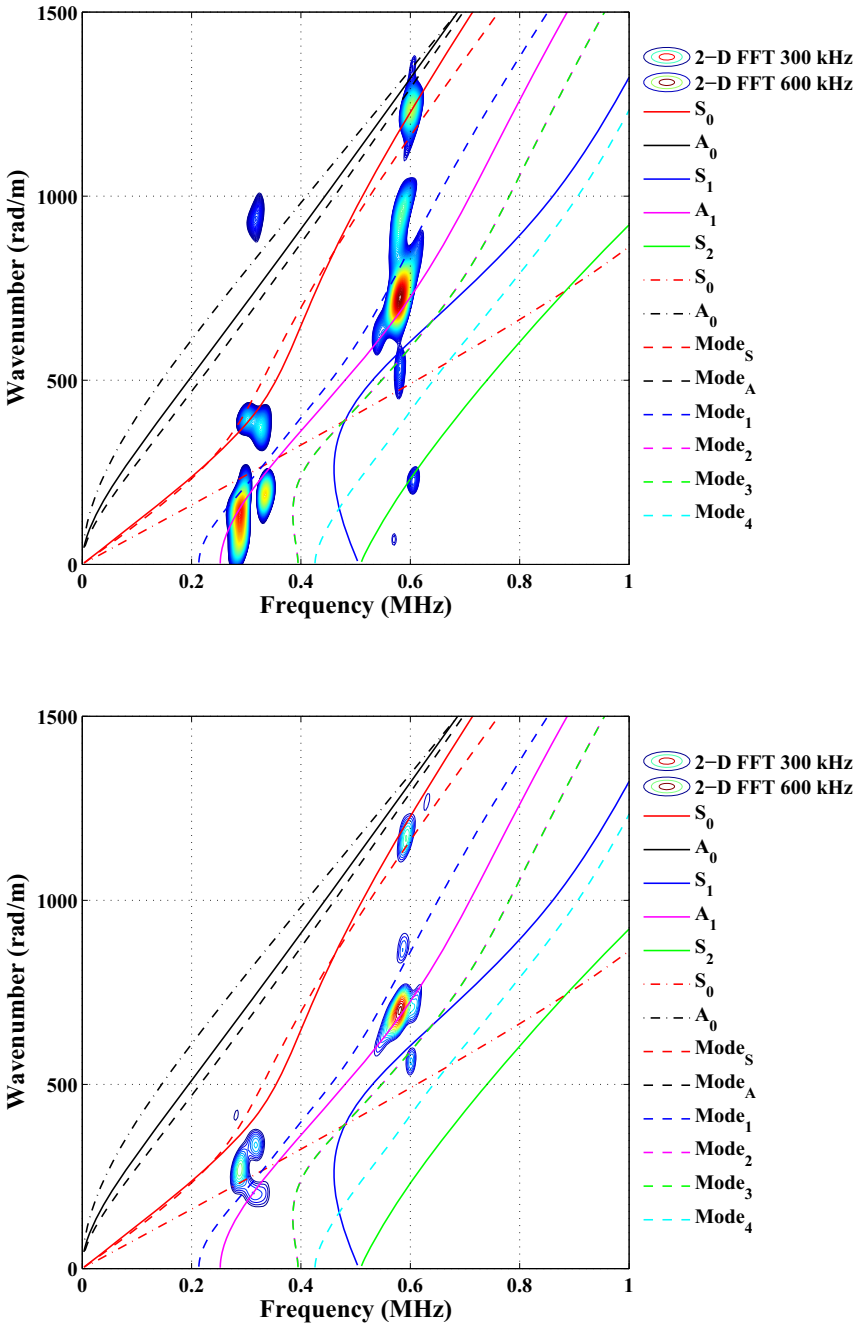

Figure 22: *As in Figure 22 but for data obtained from the patched face.*

4 Discussion

Acousto-ultrasonic measurements furnished by piezotransducer elements embedded in the bondline have been shown to provide an effective basis for the diagnostic evaluation of a metal coupon reinforced with a composite patch. The patch was shown to have a noticeable effect on the acoustic wave-field in the metal substrate, but critically this did not impair the detection of structural damage in the substrate. Indeed, a comparison of the results obtained for an identical transducer configuration on patched and unpatched samples showed that the patch fostered earlier detection of notch growth. It is surmised that the patch modifies the wavefield in a manner that accentuates interaction with the notch.

The piezoelectric transducer embedment strategy was shown to be successful. Steps were taken to ensure a thin bond line between the piezoelectric transducer and the metal substrate. A thin bond-line is thought to foster good acoustic coupling to the metallic structure, however the impact of bond-line thickness on coupling and on notch growth sensitivity was not assessed in this study. It was confirmed through laser vibrometry that substantial insonification of the patch also occurred, which is encouraging from the viewpoint of developing a diagnostic capability for the patch itself. It is to be recalled that while the objective in this work is to develop a basis for assessing defect growth in the metal substrate alone, the ultimate aim is to evolve a capability for assessing the integrity of the patch as well as the adhesive bond-line. Selective modal excitation is likely to be an important factor in achieving a targeted diagnostic capability for each of the structural elements of the repair.

While the embedment strategy was successful in fostering good defect sensitivity it is yet to be demonstrated whether embedded elements have the requisite mechanical durability to survive realistic spectrum loading. A number of issues relating to system resilience need to be addressed. For a start, the impact of an embedded stiff element on the integrity of the patch needs to be understood. Conceivably, element placement will be a critical factor, with locations within the damage tolerant zone of the patch likely to be preferred. This may require the use of a pulse-echo mode of interrogation rather than the pitch-catch approach explored in the current study.

Wiring is another key factor. Although the aim ultimately is to develop wireless strategies, the underpinning technologies are not yet mature. To this end, work has commenced on inductive and capacitive coupling strategies that could potentially eliminate the need for egress of wiring from the patch. Until the outcomes of this work are known, the development of a wired approach will continue. Routing lead wires through the composite patch rather than along the bond-line is thought advantageous in reducing the length of wiring in the installation, and more critically in eliminating an inclusion in the least damage-tolerant part of the repair. However, a potential disadvantage of a through-patch egress approach is that the necessary perforation could create a stress concentration and serve as a potential conduit for moisture ingress. Further work needs to be done to clarify the merits and disadvantages of the available wiring strategies.

Arguably, the most vulnerable aspect of wiring in an embedded sensor installation is the connection to the sensor itself, and consequently the development of a durable electrical interconnect is a key objective. A conventional soldered connection to the piezoceramic

electrode may be acceptable for laboratory work where the sample is not exposed to sustained cyclic mechanical loading, but is inadequate for any long-term in-service structural application. To address mechanical and environmental durability concerns, it is customary now to encase or package piezoelectric elements in a polymer dielectric film containing integrated conductive tracks. The commercial SMARTlayer® [8] concept follows this approach. The footprint of a single element is however quite large and poses some concern in relation to its possible impact on the structural integrity of the host. A less obtrusive packaging approach was developed recently through a collaborative effort between the DSTO and MiniFAB. The footprint of the device is only marginally larger than the piezoceramic disk element itself (see Figure 23), which serves to reduce its structural impact on the host. Trials are currently underway to assess the mechanical durability of these elements under representative aircraft spectrum loading. The preliminary results of this work are encouraging and a full account of the completed trial will be reported elsewhere.

Figure 23: *Packaged 6.35 mm diameter piezoceramic disc.*

5 Conclusion

This report has outlined the development of an "Active Smart Patch" which is a novel form of structural reinforcement that seeks to provide a diagnostic function by means of an integrated network of piezoelectric transducer elements. Experimental work has shown that a network embedded in the bondline of a composite-reinforced metal sample provides for the robust detection of damage in the metal substrate. While the laboratory demonstration was conceived to address the problem of cracking at FASS 281.28 in the F-111 wing, the technology is being developed with a much broader outlook and could potentially be applied wherever elastic waves permit an assessment of structural integrity. The F-111 problem however serves as an excellent platform for the demonstration of such technology as it embodies a number of the key challenges facing the development of an effective integrated diagnostic facility for in-flight application.

Acknowledgements

The authors gratefully acknowledge the contribution of Sami Weinberg to the development of softwares for the AUSAM and laser vibrometry facilities. The authors are also grateful to Anthony Walley, and Andrew Howard from the Australian Defence Force Academy, for their contributions to sample preparation and the experimental testing, respectively.

References

1. K. F. Walker and L. R. F. Rose. *Advances in Bonded Composite Repair of Metallic Aircraft Structure*. Elsevier, United Kingdom, 2002.

2. R. Boykett and K. F. Walker. F-111c lower wing skin bonded composite repair substantiation testing. *Defence Science and Technology Organisation, Australia*, DSTO-TR-0480, 1996.

3. S. C. Galea, S. van der Velden, I. G. Powlesland, Q. Nguyen, P. Ferrarotto, and M. Konak. Flight demonstrator of a self-powered shm system on a composite bonded patch attached to an f/a-18 aileron hinge. In *Proceedings of the First Asia-Pacific Workshop on Structural Health Monitoring (APWSHM 2006), Yokohama, Japan*, 2006.

4. A. Vary. The acousto-ultrasonic approach. Technical Memorandum 89843, NASA, 1987.

5. R. M. Rao and A. S. Bopardikar. *Wavelet Transforms - Introduction to Theory and Applications*. Addison-Wesley, Reading, Massachusetts, 1998.

6. D. N. Alleyne and P. Cawley. The interaction of lamb waves with defects. *IEEE Trans. Ultrasonics, Ferroelectrics and Frequency Control*, 39:381–397, 1992.

7. I. A. Viktorov. *Rayleigh and Lamb Waves - Physical Theory and Applications*. Plenum Press, New York, 1967.

8. Acellent Technologies Inc.

Appendix A Baseline Test Results

A.1 Unpatched Plate

SASS configuration

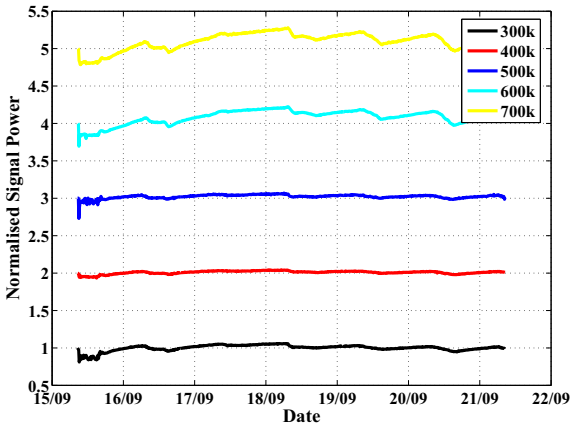

SAES configuration

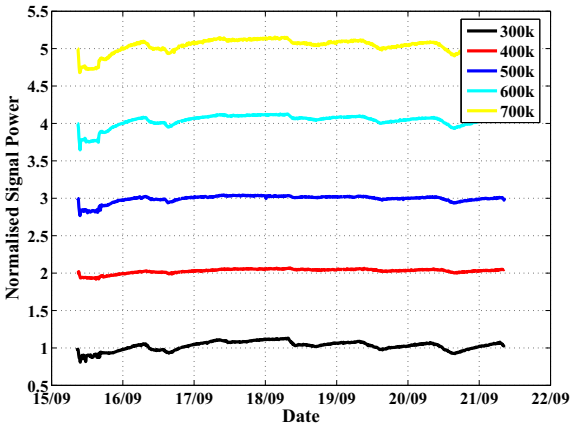

EASS configuration

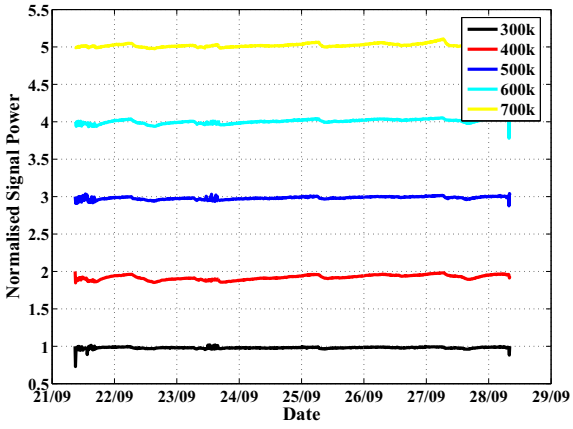

EAES configuration

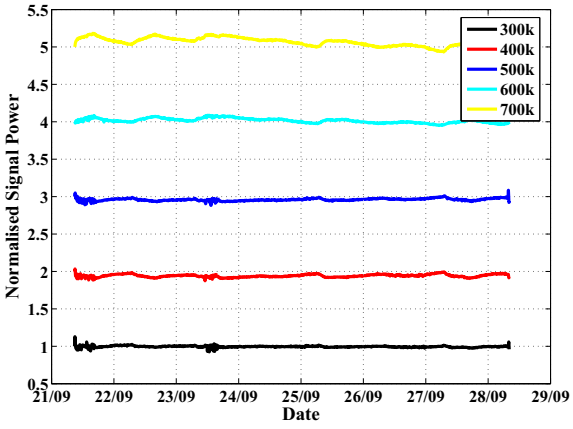

Figure A1: *Variation in signal power over time for unpatched aluminium plate; Measurements for each frequency normalised to initial signal power and shifted by unity.*

A.2 Patched Plate

SASS configuration

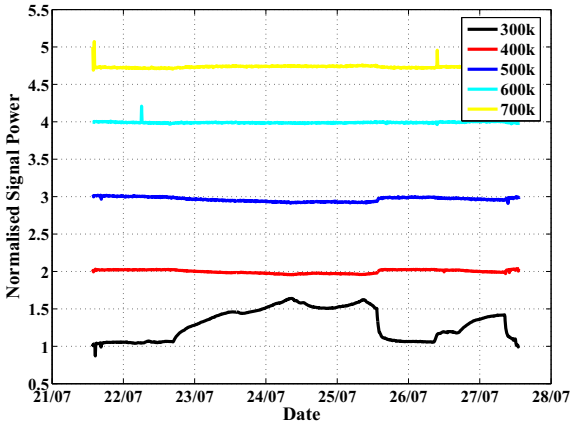

SAES configuration

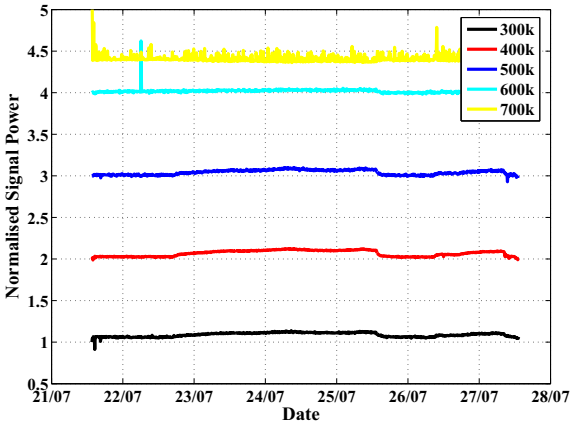

EASS configuration

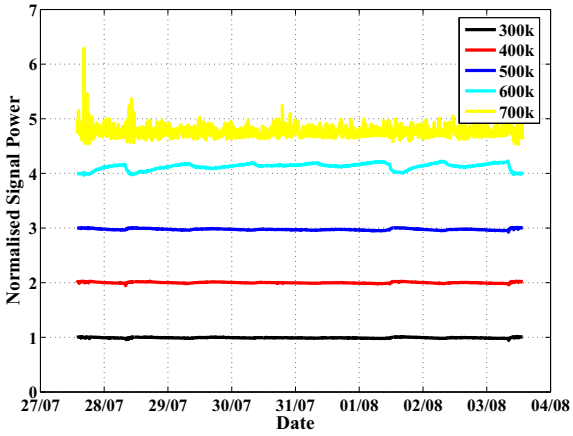

EAES configuration

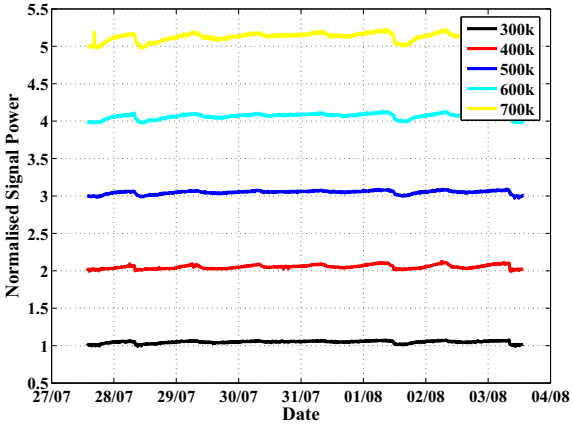

Figure A2: *As in Figure A1 but for patched aluminium plate.*

Appendix B Notch Growth Tests Results

B.1 Unpatched Plate

SASS configuration

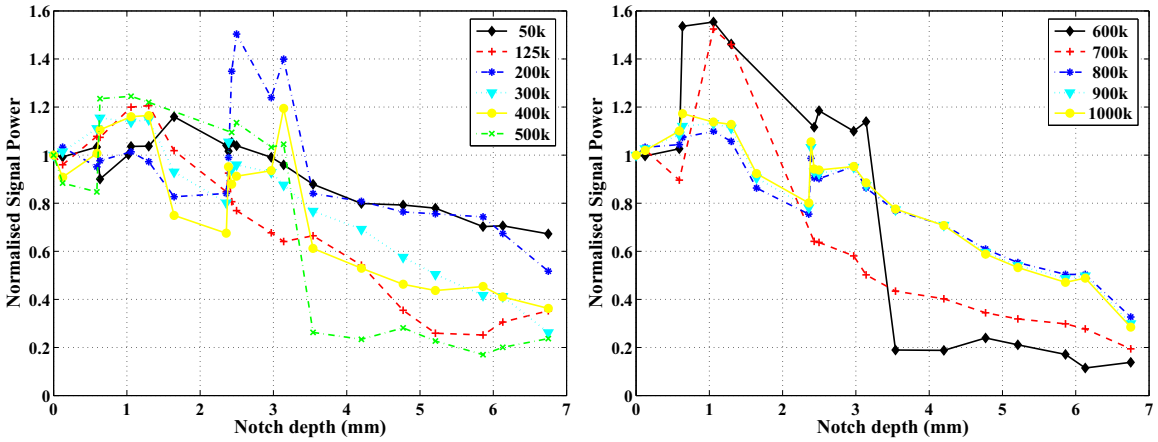

Figure B1: *Signal power measurements for the unpatched coupon in the SASS configuration.*

SAES configuration

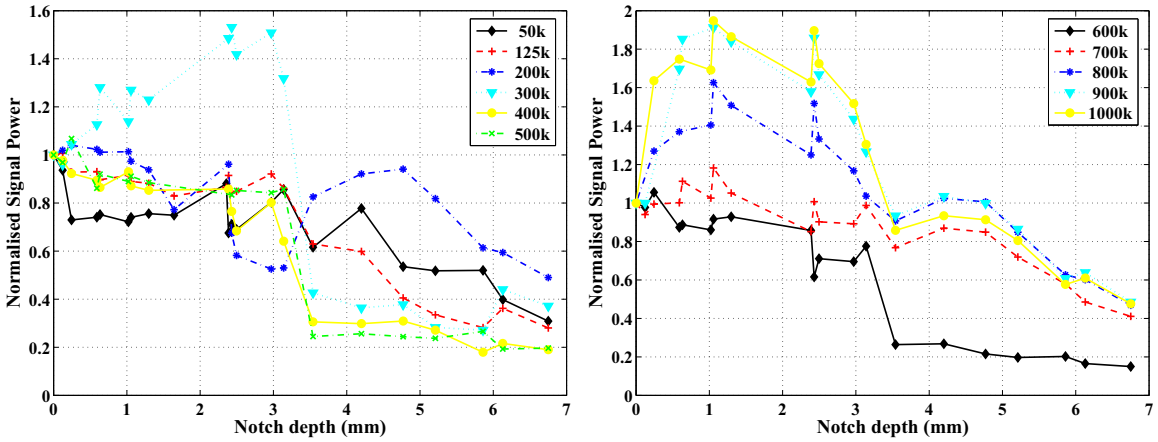

Figure B2: *As in Figure B1 but for the SAES configuration.*

EASS configuration

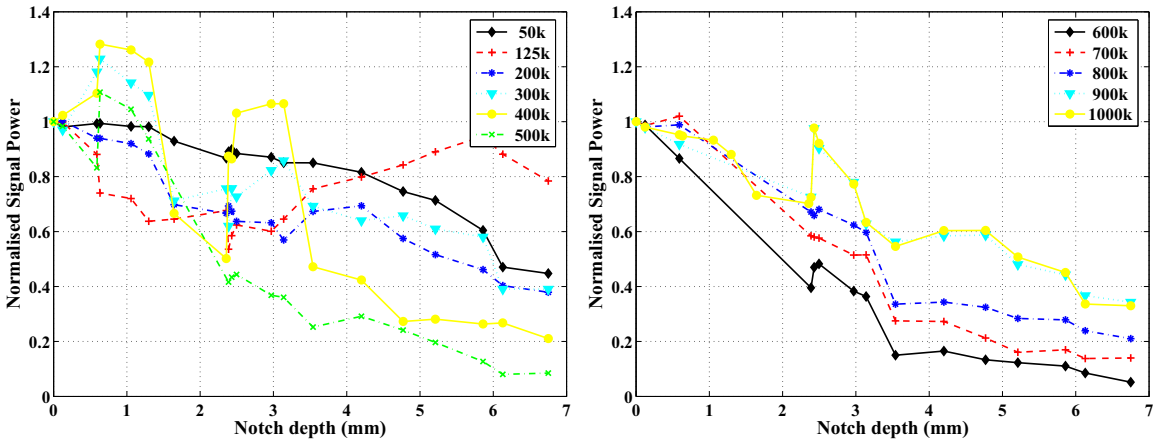

Figure B3: *As in Figure B1 but for the EASS configuration.*

EAES configuration

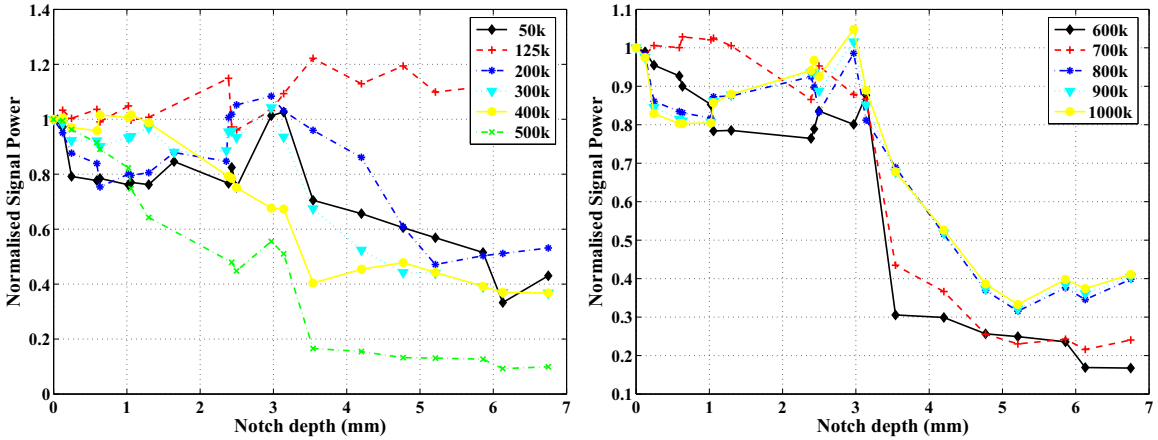

Figure B4: *As in Figure B1 but for the EAES configuration.*

B.2 Patched Plate

SASS configuration

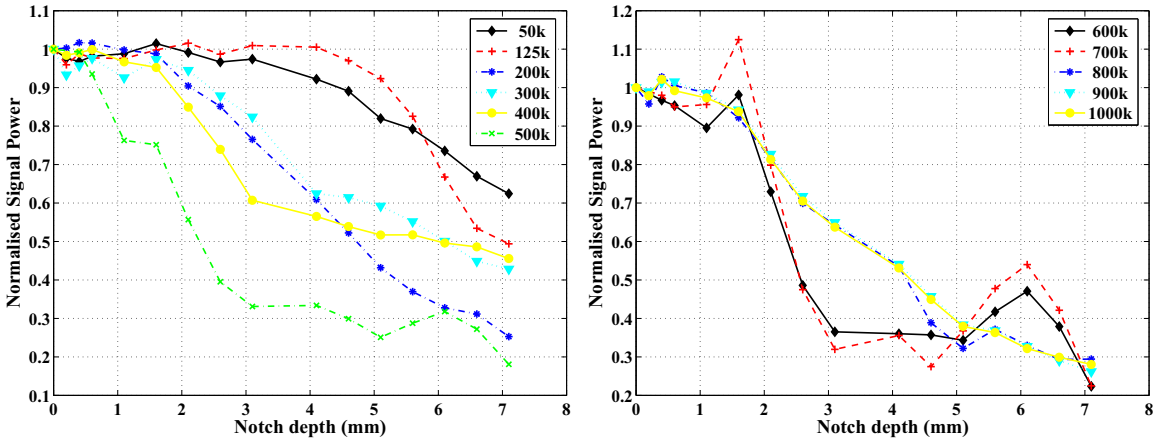

Figure B5: *As in Figure B1 but for the patched test specimen.*

SAES configuration

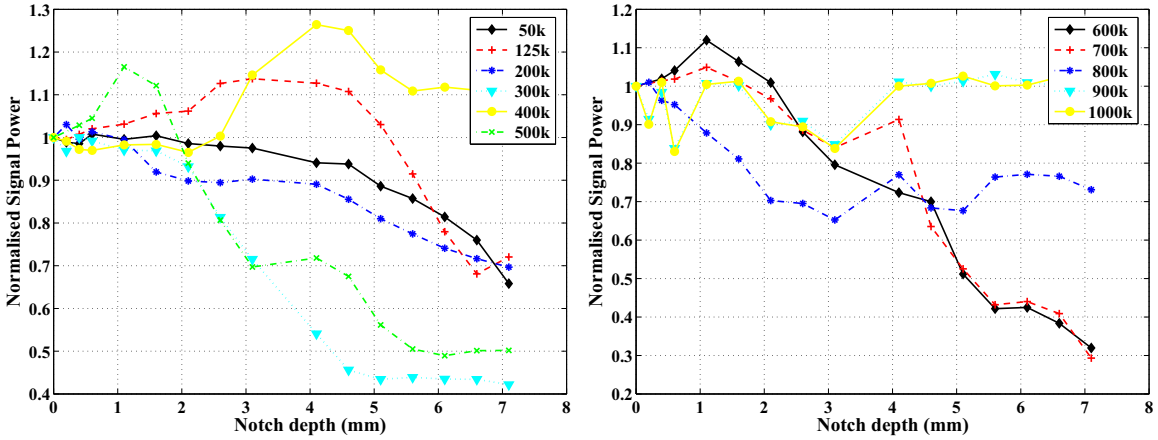

Figure B6: *As in Figure B5 but for the SAES configuration.*

EASS configuration

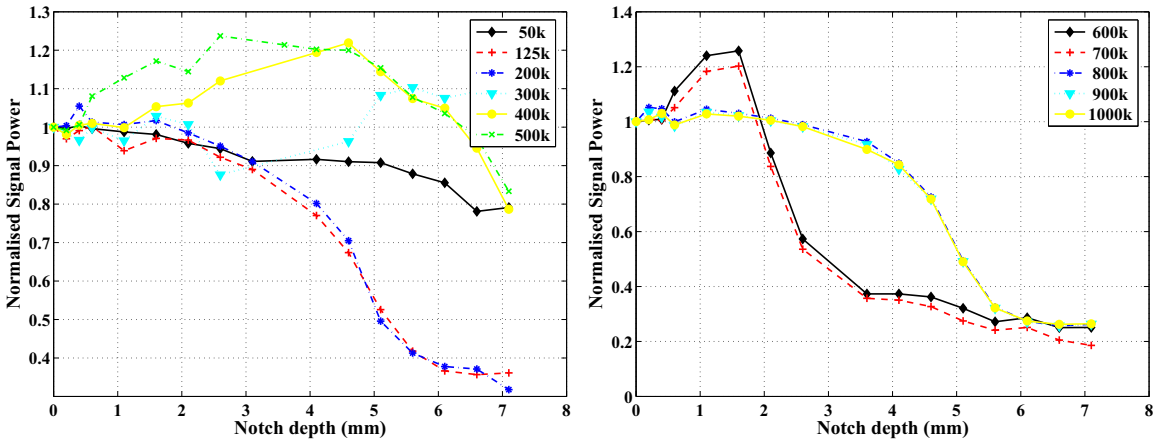

Figure B7: *As in Figure B5 but for the EASS configuration.*

EAES configuration

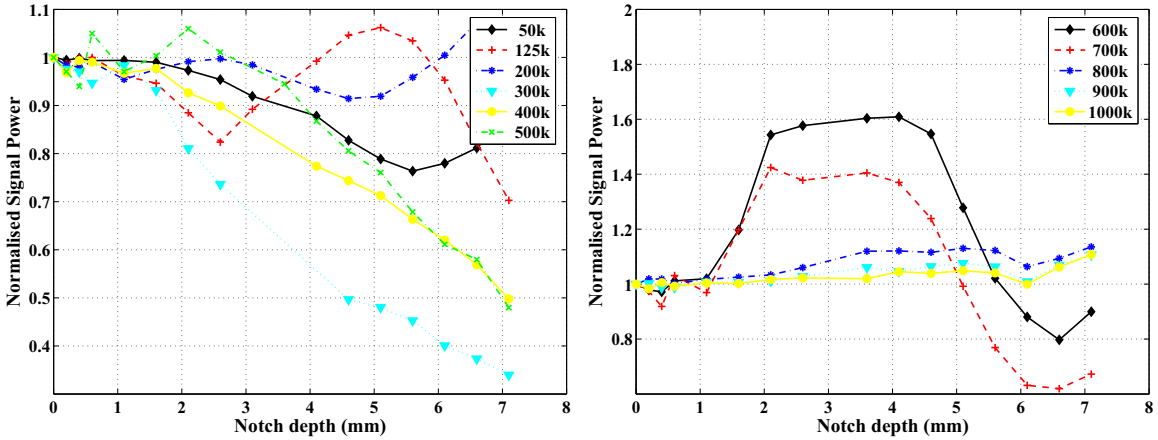

Figure B8: *As in Figure B5 but for the EAES configuration.*

Appendix C Spectral Decomposition - Unpatched Plate

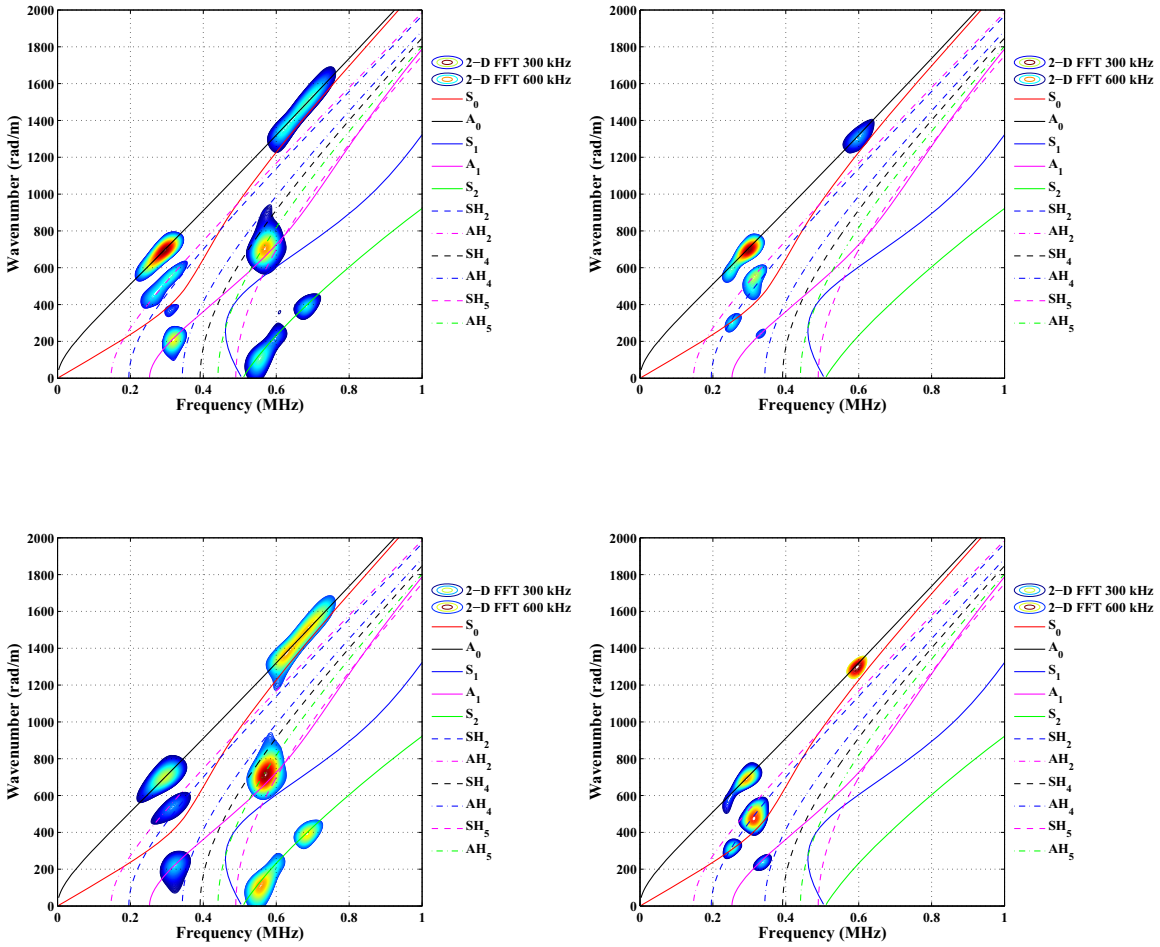

Figure C1: *Comparison of theoretical and measured dispersion characteristics, upstream (left) and downstream (right) of the notch, at two notch depths: 1.3 mm (top) and 2.36 mm (bottom). Amplitudes are normalised with respect to the peak magnitude in the upstream region for the respective excitation frequency.*

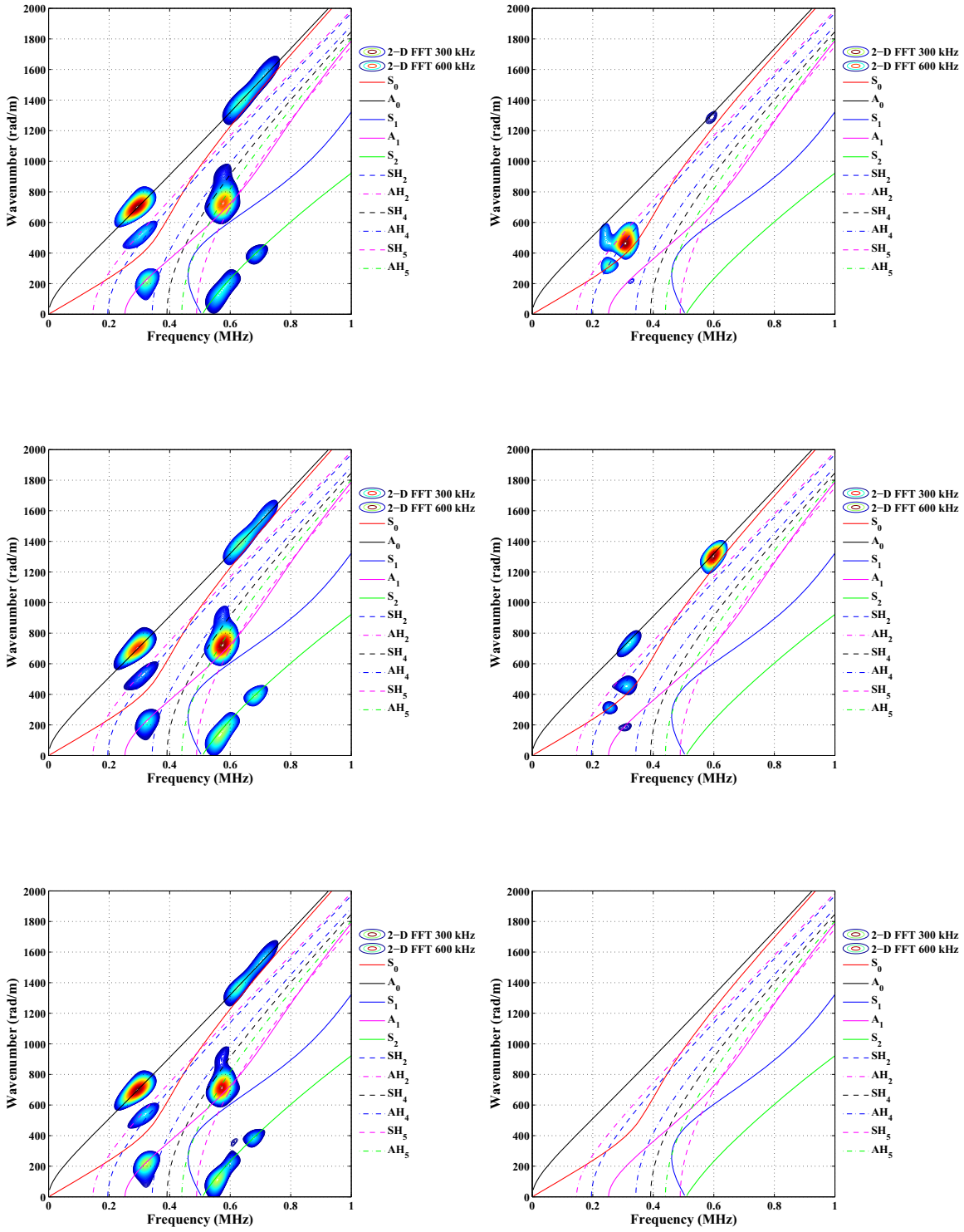

Figure C2: *As in Figure C1 but for 3.14 (top), 5.86 (middle) and 6.2 mm (bottom) notch depths.*

DEFENCE SCIENCE AND TECHNOLOGY ORGANISATION DOCUMENT CONTROL DATA	1. CAVEAT/PRIVACY MARKING

2. TITLE	3. SECURITY CLASSIFICATION
A Feasibility Study into the Active Smart Patch Concept for Composite Bonded Repairs	Document (U) Title (U) Abstract (U)
4. AUTHORS	5. CORPORATE AUTHOR
N. Rajic and S. C. Rosalie	Defence Science and Technology Organisation 506 Lorimer St, Fishermans Bend, Victoria 3207, Australia

6a. DSTO NUMBER	6b. AR NUMBER	6c. TYPE OF REPORT	7. DOCUMENT DATE
DSTO–TR–2247	014-394	Technical Report	August 2008

8. FILE NUMBER	9. TASK NUMBER	10. SPONSOR	11. No OF PAGES	12. No OF REFS
2006/1154807/1	AIR 07/053	DGTA	30	8

13. URL OF ELECTRONIC VERSION	14. RELEASE AUTHORITY
http://www.dsto.defence.gov.au/corporate/reports/DSTO–TR–2247.pdf	Chief, Air Vehicles Division

15. SECONDARY RELEASE STATEMENT OF THIS DOCUMENT

Approved For Public Release

OVERSEAS ENQUIRIES OUTSIDE STATED LIMITATIONS SHOULD BE REFERRED THROUGH DOCUMENT EXCHANGE, PO BOX 1500, EDINBURGH, SOUTH AUSTRALIA 5111

16. DELIBERATE ANNOUNCEMENT

No Limitations

17. CITATION IN OTHER DOCUMENTS

No Limitations

18. DSTO RESEARCH LIBRARY THESAURUS

Acoustic Waves, Composite Materials, F-111C, Signal Processing, Smart Materials, Smart Structures

19. ABSTRACT

This report describes an experimental investigation into a novel form of composite bonded repair called the Active Smart Patch (ASP). The ASP represents an important conceptual advancement over conventional repair technology by incorporating into a patch a network of embedded piezoelectric elements that provides a diagnostic facility for structural health. This type of repair is being developed as a means of mitigating the strict certification requirements currently placed on bonded repairs to primary aircraft structure, and as a potentially cost-efficient means of providing structural integrity assurance where lack of access precludes conventional nondestructive inspection. Initial development of the concept targets the problem of cracking at Forward Auxillary Spar Station (FASS) 281.28 in the F-111 Lower Wing Skin. As a first approximation to this problem, a prototype ASP was developed and then applied to a metal coupon which was notched to simulate cracking. The study shows that a network of piezoelectric transducers embedded in the bond-line of the patch provides a robust basis for the detection of notch growth.